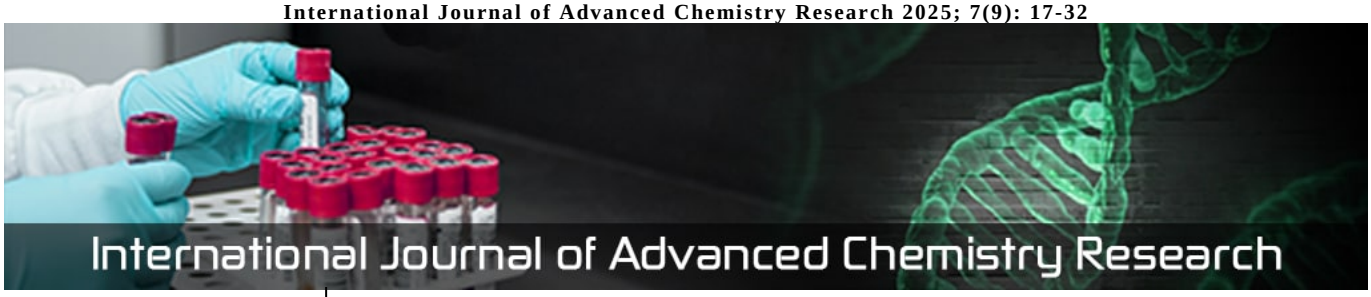


**ISSN Print:** 2664-6781
**ISSN Online:** 2664-679X
NAAS Rating (2025): 4.77
IJACR 2025; 7(9): 17-32
www.chemistryjournals.net
Received: 04-07-2025
Accepted: 06-08-2025

**Mohammad M Al-Tufah**
Directorate of Education, Kirkuk, Ministry of Education, Iraq

**Diaa M Najim**
Directorate of Education, Kirkuk, Ministry of Education, Iraq

**Corresponding Author:**
**Mohammad M Al-Tufah**
Directorate of Education, Kirkuk, Ministry of Education, Iraq

# Synthesis and docking-based evaluation of mannich derivatives targeting estrogen receptors in mcf-7 cells and evaluation of antibacterial activity

**Mohammad M Al-Tufah and Diaa M Najim**

**DOI:** https://www.doi.org/10.33545/26646781.2025.v7.i9a.310

**Abstract**
The persistent rise in antimicrobial resistance and the growing burden of chemo-resistant breast cancer have driven the need for dual-acting therapeutic agents. In this study, four novel Mannich base derivatives ($N_1$-$N_4$) were synthesized via a classical one-pot condensation of 4-ethoxyacetophenone with different substituted secondary amines. The structures were confirmed through FTIR, $^1$H-NMR, and $^{13}$C-NMR spectral analysis. Antibacterial activity was evaluated using the agar well diffusion method against *Staphylococcus aureus* and *Escherichia coli*, while cytotoxicity against the MCF-7 breast cancer cell line was assessed using the MTT assay. Notably, compounds $N_2$ and $N_3$ demonstrated moderate to strong antibacterial activity, with $N_2$ showing 20 mm and 18 mm inhibition zones against *S. aureus* and *E. coli*, while $N_3$ recorded 16 mm and 14 mm, respectively, at 0.1 mg/mL. In contrast, $N_1$ and $N_4$ exhibited potent cytotoxic effects, with $IC_{50}$ values of 18.7 µg/mL and 21.3 µg/mL, respectively. Furthermore, molecular docking of $N_1$ with the estrogen receptor alpha (PDB: 5T92) revealed stable binding with a docking affinity of -7.73 kcal/mol, supported by favorable hydrogen bonding and hydrophobic interactions with MET421 and PHE404. These results suggest that specific substitutions on the amine moiety significantly influence biological activity, either through enhanced cellular uptake or better receptor binding. Overall, this study confirms that structural tuning of Mannich bases can yield promising multifunctional compounds, potentially overcoming the limitations of single-target therapies. Future research may further optimize these derivatives for selectivity, bioavailability, and *in vivo* efficacy.

**Keywords:** Antibacterial, anticancer, breast cancer (mcf-7), cytotoxicity, docking, estrogen receptor, mannich base

## Introduction
The emergence and rapid spread of antimicrobial resistance among pathogenic bacteria have posed a profound threat to global public health. As conventional antibiotics lose their effectiveness, infections caused by drug-resistant strains of *Escherichia coli* and *Staphylococcus aureus* have become increasingly challenging to treat [1]. Consequently, researchers have redirected their attention toward designing novel hybrid molecules with enhanced antimicrobial profiles [2]. Simultaneously, cancer remains a leading cause of mortality worldwide, and among the various types, breast cancer, particularly the MCF-7 subtype, has shown significant resistance to many chemotherapeutic agents. As a result, there is a growing demand for the development of multifunctional compounds that can exert dual biological activities, ideally serving as both antibacterial and anticancer agents [3]. Mannich bases, which are β-amino carbonyl compounds typically synthesized via the condensation of a carbonyl compound, an amine, and formaldehyde, have attracted considerable interest in medicinal chemistry [4]. This interest stems from their structural versatility, synthetic accessibility, and broad spectrum of biological activities. It is well established that incorporating nitrogen-containing groups into drug scaffolds often enhances their pharmacological potential [5]. Furthermore, recent studies have demonstrated that Mannich bases exhibit promising antibacterial, antifungal, anti-inflammatory, and anticancer activities. Due to their ability to interact with microbial enzymes and DNA through hydrogen bonding

and π-π stacking, these compounds can disrupt vital cellular processes, leading to the death of microbial or cancer cells [6]. Despite the therapeutic potential of Mannich bases, limited studies have explored their dual activity against both bacterial pathogens and cancer cell lines in a single compound series [7]. This research gap underscores the need to design and synthesize novel Mannich base derivatives and evaluate their bioactivities using both microbiological and cell-based assays. Addressing this gap could provide valuable insights into structure, activity relationships and identify lead compounds with potential for further development [8].

This study aims to assess the antibacterial and anticancer potential of newly synthesized Mannich base derivatives $N_1$-$N_4$. By developing a synthetic route using acetophenone, formaldehyde, and diverse secondary amines, we analyze how chemical structure influences biological effects. Antibacterial efficacy is tested against *E. coli* and *S. aureus*, while anticancer potential is investigated using the MCF-7 cell line. Through FTIR and NMR characterizations, coupled with molecular docking and *in vitro* assays, this research explores key structure-activity relationships. Ultimately, the findings may identify lead molecules with dual activity for future drug development targeting both microbial and cancer-related pathways.

## Materials and Methods

Chemicals have been purchased from Sigma-Aldrich (USA) and BDH Chemicals (UK). Purchased reagents included: -Hydroxyacetophenone, N-methyl-4-aminophenol, 4-ethyl-N-methylaniline, N-methyl-p-toluidine, N-methylaniline, dimethyl sulfoxide (DMSO), Acetone, Ethyl iodide, $K_2CO_3$, formaldehyde solution (37% w/w), tetrahydrofuran (THF), ethyl acetate, ethanol (absolute), chloroform, and all basic laboratory consumables, and all basic laboratory consumables. Muller-Hinton agar was also acquired from Sigma-Aldrich and used as the standard growth medium for antimicrobial assays. All glassware was sterilized, and aseptic procedures were observed.

### Synthesis of 4-Ethoxy acetophenone (A). [9]

Hydroxyacetophenone (1.36 g, 0.01 mol) was dissolved in 25 mL of dry acetone. Anhydrous potassium carbonate (2.76 g, 0.02 mol) was added, followed by the dropwise addition of ethyl iodide (1.0 ml, 0.01 mol). The mixture was refluxed at 65°C for 6 hours. After cooling, the mixture was filtered, and the filtrate was poured into water. The solution was extracted with ethyl acetate (3 × 20 mL). The combined organic layers were washed with saturated brine, dried, and concentrated. The crude product was purified by recrystallization from ethanol, affording 4-ethoxyacetophenone as a pale-yellow oil in 70-75% yield.

### Synthesis of Mannich Base Derivatives ($N_1$-$N_4$). [10]

4- ethoxyacetophenone (1.64 g, 0.01 mol) was dissolved in 20 mL of tetrahydrofuran (THF) under continuous stirring at room temperature. Four parallel reactions were carried out using different amine precursors. In the first reaction, N-methyl-p-toluidine (1.21 g, 0.01 mol) was added to the solution, while in the other three reactions, N-methyl-4-aminophenol (1.23 g, 0.01 mol), 4-ethyl-N-methylaniline (1.35 g, 0.01 mol), and N-methylaniline (1.07 g, 0.01 mol) were introduced under identical conditions. After complete dispersion of the amines, (0.3 g, 0.01 mol) 37 % of formaldehyde was added dropwise to each reaction mixture with continuous stirring. The mixtures were stirred at room temperature for 1 hour and then heated under gentle reflux on a steam bath for 20 minutes. The mixtures were cooled to room temperature and stored at 4 °C for 48 hours to allow for full crystallization. The resulting solid precipitates N1-N4 were collected by filtration, washed thoroughly with cold distilled water, and purified via recrystallization from a 1:1 (v/v) ethanol and chloroform mixture. The physical properties of the derivatives of Mannich bases ($N_1$-$N_4$) are shown in Table 1.

**Table 1:** Physical constants of Mannich Base Derivatives ($N_1$-$N_4$).

| Compound No. | X | Structural formula | M. wt (g/mol) | M.P. (°C) | Yield % | Colour |
|---|---|---|---|---|---|---|
| **$N_1$** | $CH_3$ | $C_{19}H_{23}NO_2$ | 297.4 | 256 | 65 | light yellow |
| **$N_2$** | OH | $C_{18}H_{21}NO_3$ | 299.3 | 278 | 54 | brown |
| **$N_3$** | $C_2H_5$ | $C_{20}H_{25}NO_2$ | 311.4 | 263 | 68 | light yellow |
| **$N_4$** | H | $C_{18}H_{21}NO_2$ | 283.3 | 243 | 72 | yellow |

### Antibacterial effect study

The antimicrobial activity of the synthesized Mannich base derivatives ($N_1$-$N_4$) was evaluated using the cup-plate agar diffusion method, and the inhibition zones were measured in millimeters. The compounds were tested at three different concentrations (0.01, 0.001, and 0.0001) mg/mL, which served as the reference drug. Antibacterial activity was assessed against two clinically relevant bacterial strains: *Staphylococcus aureus* and *Escherichia coli*. The micro-organisms have been isolated and identified at Medical Laboratory Techniques Department/ Technical College in Kirkuk. Muller-Hinton agar was used as the culture medium for all microbiological testing [11]. Ciprofloxacin was employed as a standard medication to investigate these compounds' possible actions. Using a loop, the test compounds were injected into plates containing Nutrient Agar (NA) medium, and they were then brooded for 24 hours at 37°C. Prepared bacterial suspensions in distilled water were used to perform the agar diffusion. Every other compound that was analyzed was contrasted with the substances that were being tested. To evaluate the synthetic compounds' antibacterial properties, the widths of the inhibitory zones surrounding each well were determined in millimeters after incubation [12].

### Molecules Docking Preparation

The novel derivative ($N_1$) was synthesised and characterised using Chemdraw Ultra 12.0 (https://chemdraw pro.software.informer.com/12.0/) program to create its 3D structure and energy minimization. Using Hyperchem 8.08, semi-empirical AM1 pre-optimized the structures [13]. Using the B3LYP/6-31G basis set, density functional theory DFT optimised the structures for the most stable conformation [14]. By default, maximum force, root-mean-square (RMS) force, maximum displacement, values are positive, indicating stability. The optimised structures were merged in

one database using MOE software (Molecular Operating Environment (MOE), 2019) to analyse ligand affinity [15].

**Receptor preparation**

The Protein Data Bank's crystal structure of the oestrogen receptor alpha ligand binding domain in complex with (PDB ID: 5T92)[16] (Scheme 1) was chosen. Because the water molecule at the target enzyme's active site is critical, it was introduced to establish a hydrogen connection between the ligand and target. Next, the protein structure was produced by repairing the missing bonds broken in X-ray diffraction and adding hydrogen atoms. Importantly, PDB is a reliable source for biological macromolecule crystal structures globally. The Oestrogen Receptor alpha (ERα) ligand-binding domain, 5T92, is critical for the development and progression of oestrogen receptor-positive ($ER^+$) breast cancer. When ERα binds to oestrogen, it activates genes involved in cell growth and survival. In hormone-dependent breast cancer, ERα overexpression or activation leads to uncontrolled cell proliferation, making it a crucial therapeutic target. A well-characterized binding location and importance to hormone-driven breast cancer led to its selection for molecular docking, enabling in silico screening of putative ERα antagonists [17-18].

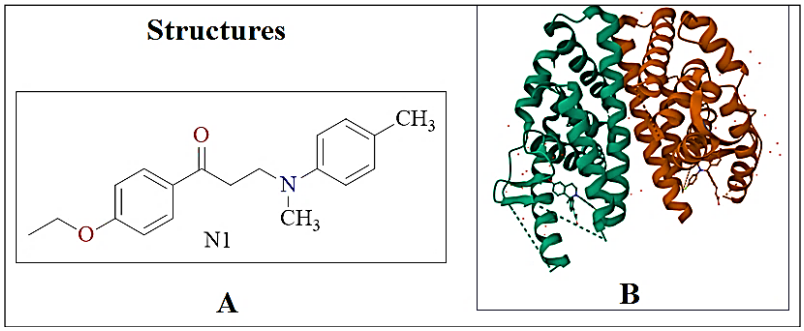


**Scheme 1:** Ligand with protein, A: Chemical structures of ligand N1, B: of Crystal structures the 5T92 protein

**Ligand-Protein molecular docking**

MOE was used for all docking and scoring computations (Molecular Operating Environment, 2019) [19]. The Protein Data Bank provided the crystal structure of the Oestrogen Receptor Alpha Ligand Binding Domain in Complex with (PDB ID: 5T92) (Scheme 2) at a resolution of 2.22 Å. A resolution of 1.5 to 2.5 Å is suitable for docking investigations. The optimal RMSD score is about 2 Å with an energy score below -7 kcal/mol. Both of these measurements are typically used to confirm molecular docking results [20].

**Results and Discussion**

The sequence shown in Scheme 2 was used to synthesize the compounds:

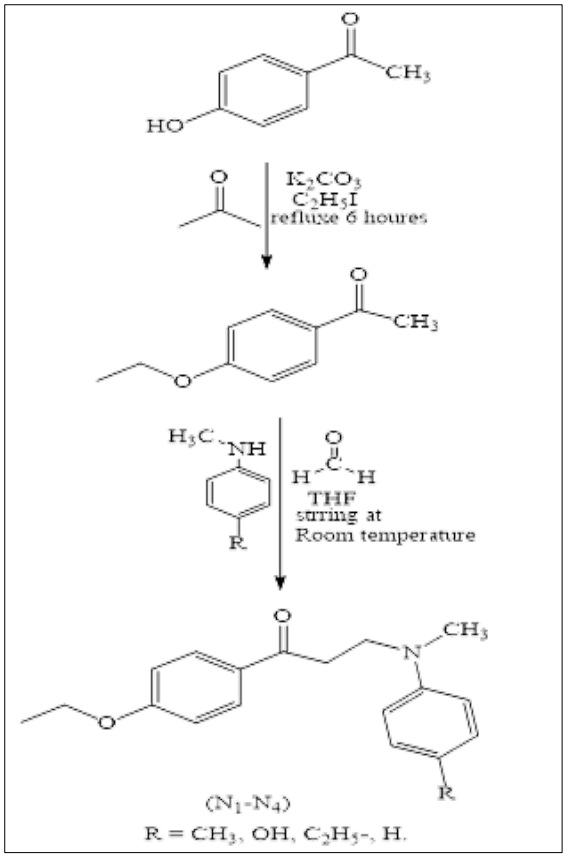


**Scheme 2:** Synthesis Pathway of Mannich bases ($N_1$-$N_4$).

**Characterization of compounds ($N_1$-$N_4$)**

Compounds ($N_1$-$N_4$) were produced by reacting 4-ethoxyacetophenone with substituted aromatic amines and formaldehyde in the presence of THF, as shown in Scheme 3.

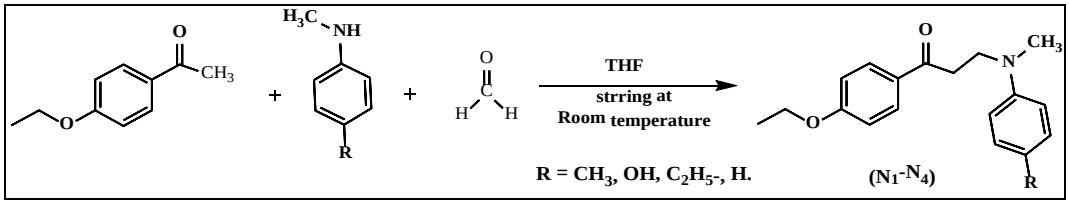


**Scheme 3:** Preparation of Mannich bases ($N_1$-$N_4$).

In theMannich reaction, a primary or secondary amine condenses with formaldehyde and a molecule that has at least one highly reactive hydrogen atom. The reaction's primary characteristic is the substitution of an aminomethyl or substituted aminomethyl group for the active hydrogen atom. One example is the mixture of formaldehyde, acetophenone, and a secondary amine salt [21]. The suggested reaction mechanism is illustrated in Scheme 4.

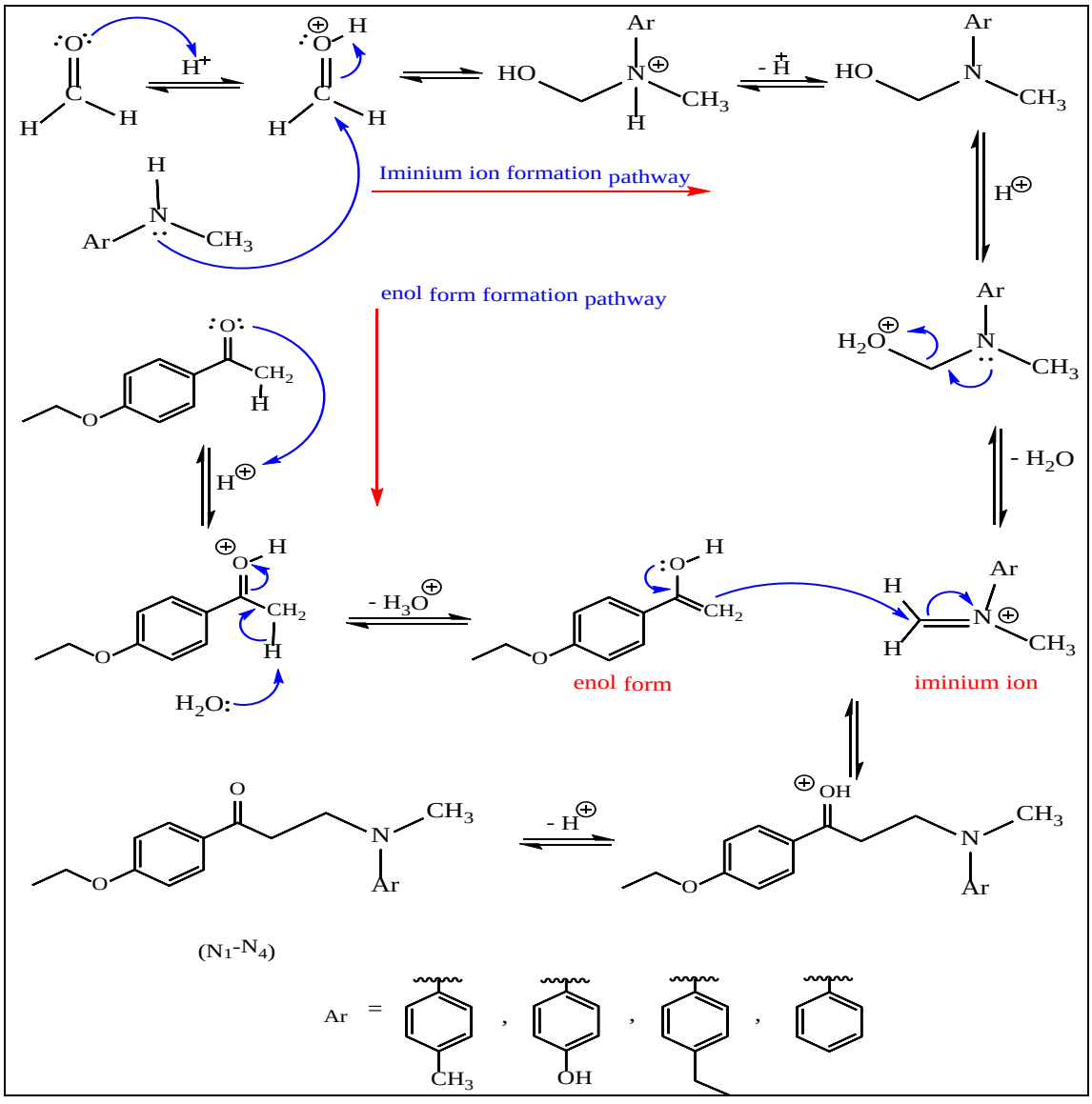


Scheme 4: Mechanism of Mannich bases synthesis (N1-N4).

The synthesized Mannich base derivatives ($N_1$-$N_4$) are confirmed through characteristic FTIR, $^1$H-NMR and $^{13}$C-NMR spectral features consistent with the proposed structures.

The FTIR (cm-1) spectra for synthesis derivatives $N_1$-$N_4$ are shown in Table 2 and Figures 1-4. The prepared derivative $N_1$ was characterized by the infrared spectrum, as it showed an absorption band within the IR: 3105 cm$^{-1}$, 2923 cm$^{-1}$, 1692 cm$^{-1}$, 1251 cm$^{-1}$, and 1206 cm$^{-1}$, indicating the υ(C-H) aromatic stretching vibration, υ(C-H) aliphatic, υ(C=O) of ketone group, (C-O), and υ(C-N), respectively [22]. The absorption spectrum in the infrared spectrum was also used

to describe the resulting derivative $N_2$. The IR spectrum showed 3594 $cm^{-1}$, 3079 $cm^{-1}$, 2963 $cm^{-1}$, 1692 $cm^{-1}$, 1305 $cm^{-1}$, and 1188 $cm^{-1}$, indicating the υ(O-H), υ(C-H) aromatic stretching vibration, υ(C-H) aliphatic, υ(C=O) of ketone group, (C-O), and υ(C-N), respectively [23]. While the IR absorption spectrum of the resulting derivative $N_3$ showed 2925 $cm^{-1}$, 1697 $cm^{-1}$, 1260 $cm^{-1}$, and 1007 $cm^{-1}$, indicating the υ(C-H) aliphatic stretching vibration, υ(C=O) of the ketone group, (C-O), and υ(C-N), respectively [24]. The FTIR ($cm^{-1}$) of derivative $N_4$ shows bands at: 3099 $cm^{-1}$, 2950 $cm^{-1}$, 1686 $cm^{-1}$, and 1278 $cm^{-1}$, indicating the υ(C-H) aromatic stretching vibration, υ(C-H) aliphatic, υ(C=O) of the ketone group, and (C-O), respectively [25].

**Table 2:** FT-IR data of synthesized Mannich bases derivatives ($N_1$-$N_4$)

| Compound No. | υ (C-H) Aromatic | υ (C-H) Aliphatic (Sym., Asy.) | υ (C=O) | υ (C=C) Aromatic (Sym., Asy.) | υ (C-O) | Other absorptions |
|---|---|---|---|---|---|---|
| $N_1$ | 3105 | 2923, 2857 | 1692 | 1629, 1451 | 1206 | υ (C-N) 1188 |
| $N_2$ | 3079 | 2963, 2824 | 1685 | 1596, 1495 | 1251 | υ (O-H) 3594 |
| $N_3$ | 3035 | 2925, 2837 | 1697 | 1617, 1535 | 1260 | υ (C-N) 1007 |
| $N_4$ | 3099 | 2950, 2845 | 1686 | 1617, 1582 | 1278 | υ (C-N) 1184 |

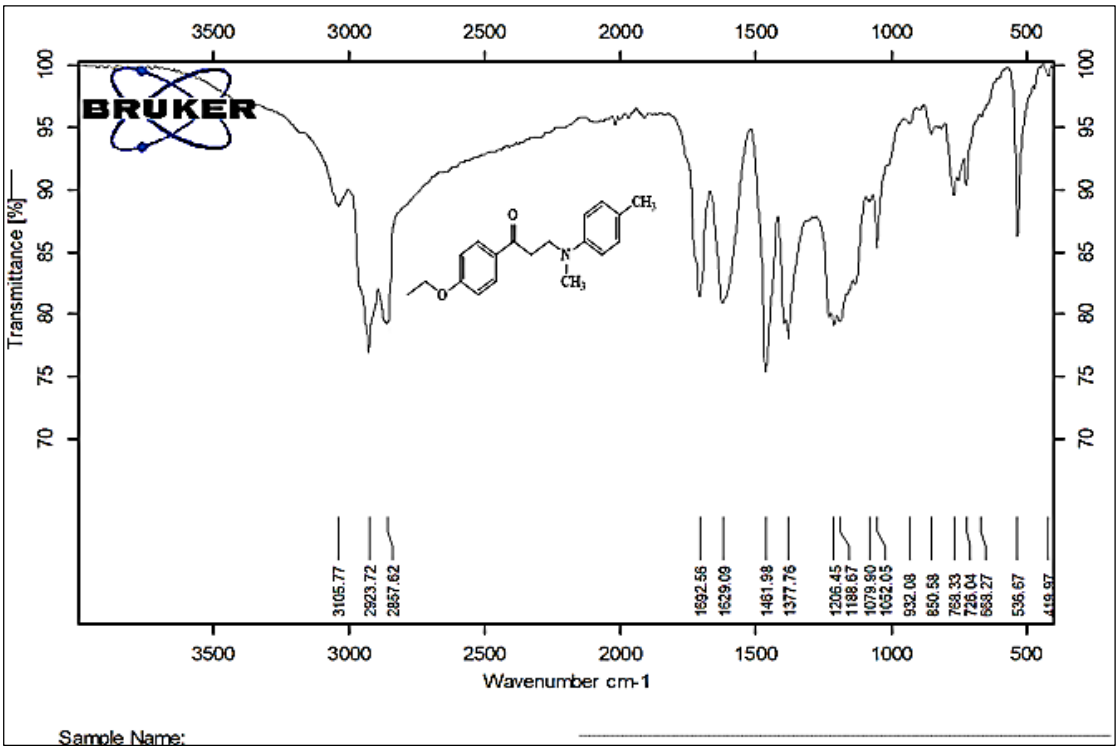


**Fig 1:** FTIR spectrum of derivative $N_1$.

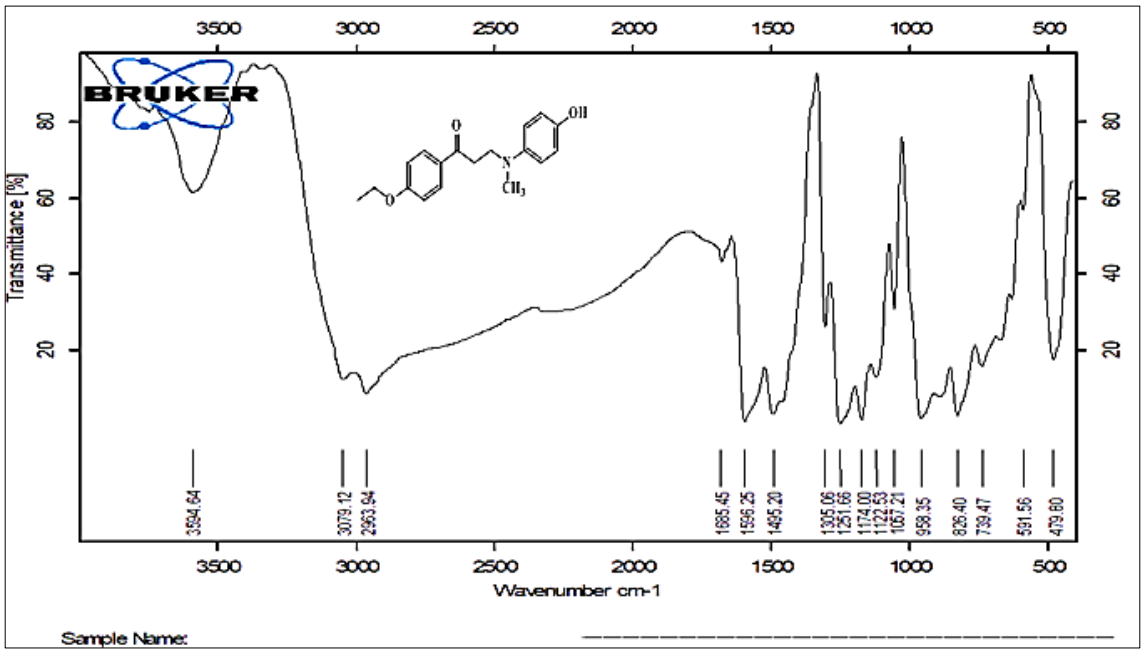


**Fig 2:** FTIR spectrum of derivative N2.

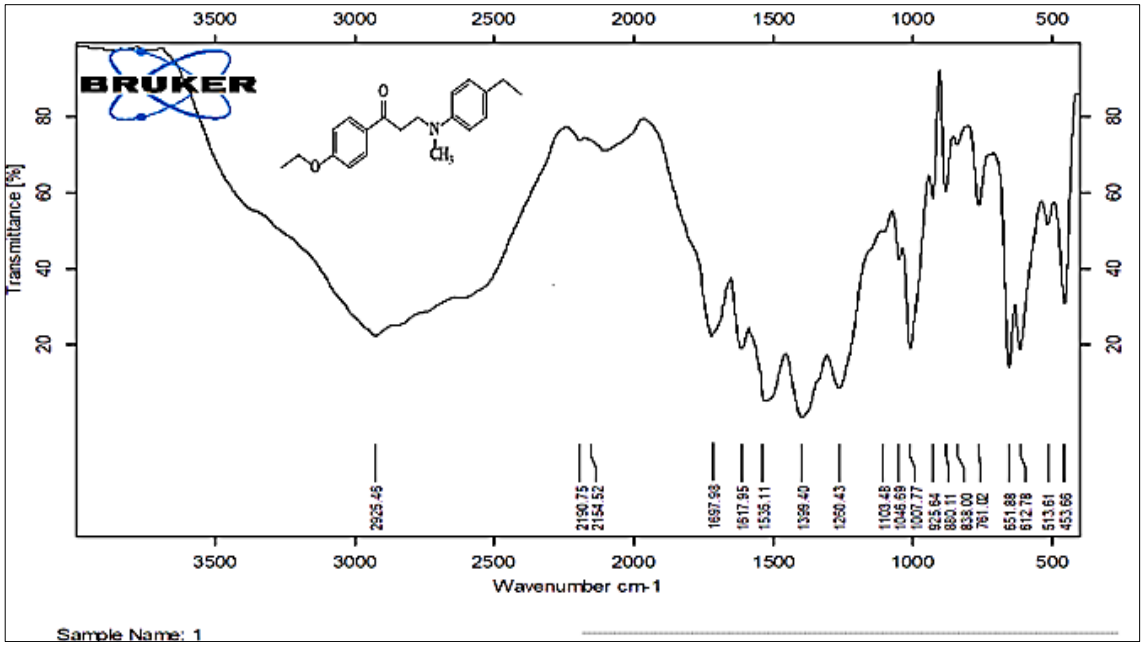


**Fig 3:** FTIR spectrum of derivative N3.

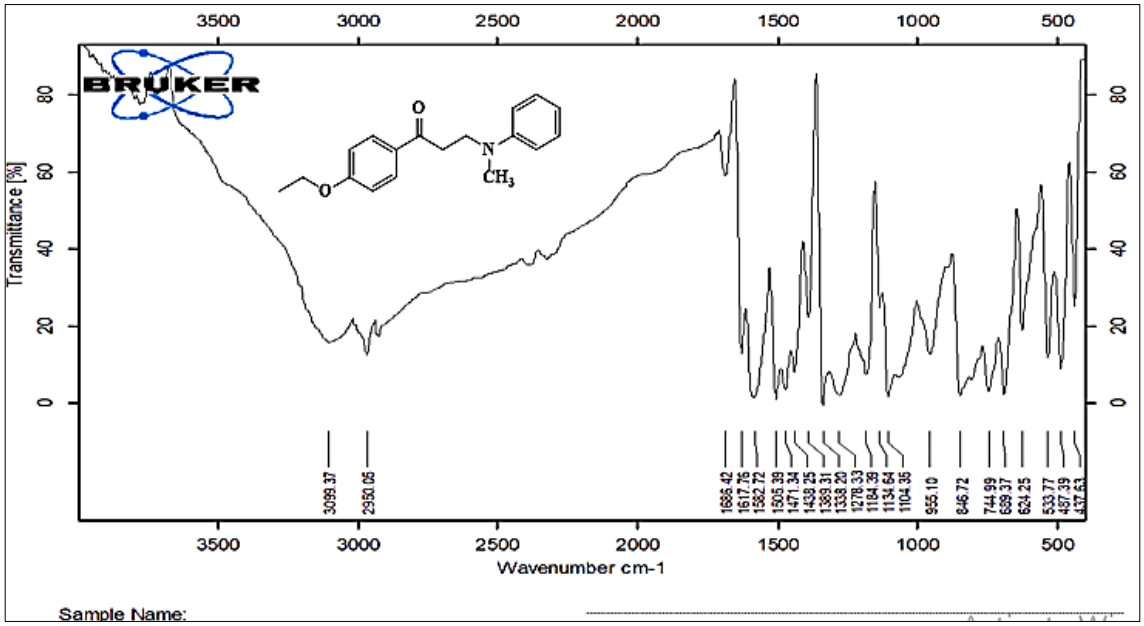


**Fig 4:** FTIR spectrum of derivative $N_4$.

**Discussion of ($^1$H-NMR and $^{13}$C-NMR) spectra**

Using tetramethylsilane as an internal reference, the 1H-NMR and 13C-NMR spectra were obtained in DMSO using a 400 MHz spectrometer.

The derivative $N_1$: $^1$H-NMR (400 MHz, DMSO) δ, 7.26-8.0 showed as (multiplet, 8H, Aromatic ring), 4.01-4.05 as (tetra, 2H, O-$CH_2$), 3.01 (singlet, 3H, N-$CH_3$), 3.19-3.21 as two (doublet, 2H, methylene), while 1.42-1.45 (triplet, 3H, methyl) and 1.60 (singlet, 3H, methyl) [26]. The derivative $N_2$: $^1$H-NMR (400 MHz, DMSO) δ, 9.30 (s, 1H, hydroxyl), 6.99-7.59 showed as (multiplet, 8H, Aromatic ring), 4.07-4.14 as (tetra, 2H, O-$CH_2$), 2.88 (singlet, 3H, N-$CH_3$), 3.15-3.40 as two (doublet, 2H, methylene), while 1.25-1.28 (triplet, 3H, methyl) [27]. The derivative $N_3$: $^1$H-NMR (400 MHz, DMSO) δ, 7.63-8.15 showed as (multiplet, 8H, Aromatic ring), 4.12-4.14 as (tetra, 2H, O-$CH_2$), 2.66-2.98 as (tetra, 2H, methylene), 3.19-3.21 as (triplet, 2H, methylene), while 1.25-1.28 and 1.44-1.47 (triplet, 3H, methyl) and 3.18 (singlet, 3H, N-$CH_3$) [28]. The derivative $N_4$: $^1$H-NMR (400 MHz, DMSO) δ, 7.26-8.0 showed as (multiplet, 8H, Aromatic ring), 4.01-4.05 as (tetra, 2H, O-$CH_2$), 3.01 (singlet, 3H, N-$CH_3$), 3.19-3.21 as two (doublet, 2H, methylene), while 1.42-1.45 (triplet, 3H, methyl) and 1.60 (singlet, 3H, methyl) [29]. Note Figures 5-7.

The derivative $N_1$: $^{13}$C-NMR (400 MHz, DMSO) δ, 194 for carbon of carbonyl group, 113-161 for carbons of aromatic rings, 65 and 73 for methylene that connect with O and N, 19 and 21 for carbons of methyl groups [30]. The derivative $N_2$: $^{13}$C-NMR (400 MHz, DMSO) δ, 194 for carbon of carbonyl group, 115-161 for carbons of aromatic rings, 51 and 65 for methylene that connect with O and N, 25 and 36 for carbons of methyl groups. The derivative $N_3$: $^{13}$C-NMR (400 MHz, DMSO) δ, 192 for carbon of carbonyl group, 112-172 for carbons of aromatic rings, 54 and 67 for methylene that connect with O and N, 50 for methyl connect with N, 19 and 21 for carbons of methyl groups,. The

derivative $N_4$: $^{13}$C-NMR (400 MHz, DMSO) δ, 194 for carbon of carbonyl group, 112-167 for carbons of aromatic rings, 54 and 67 for methylene that connect with O and N, 48 for methyl connected with N, 21 for carbons of methyl groups. Note Figures 8-10.

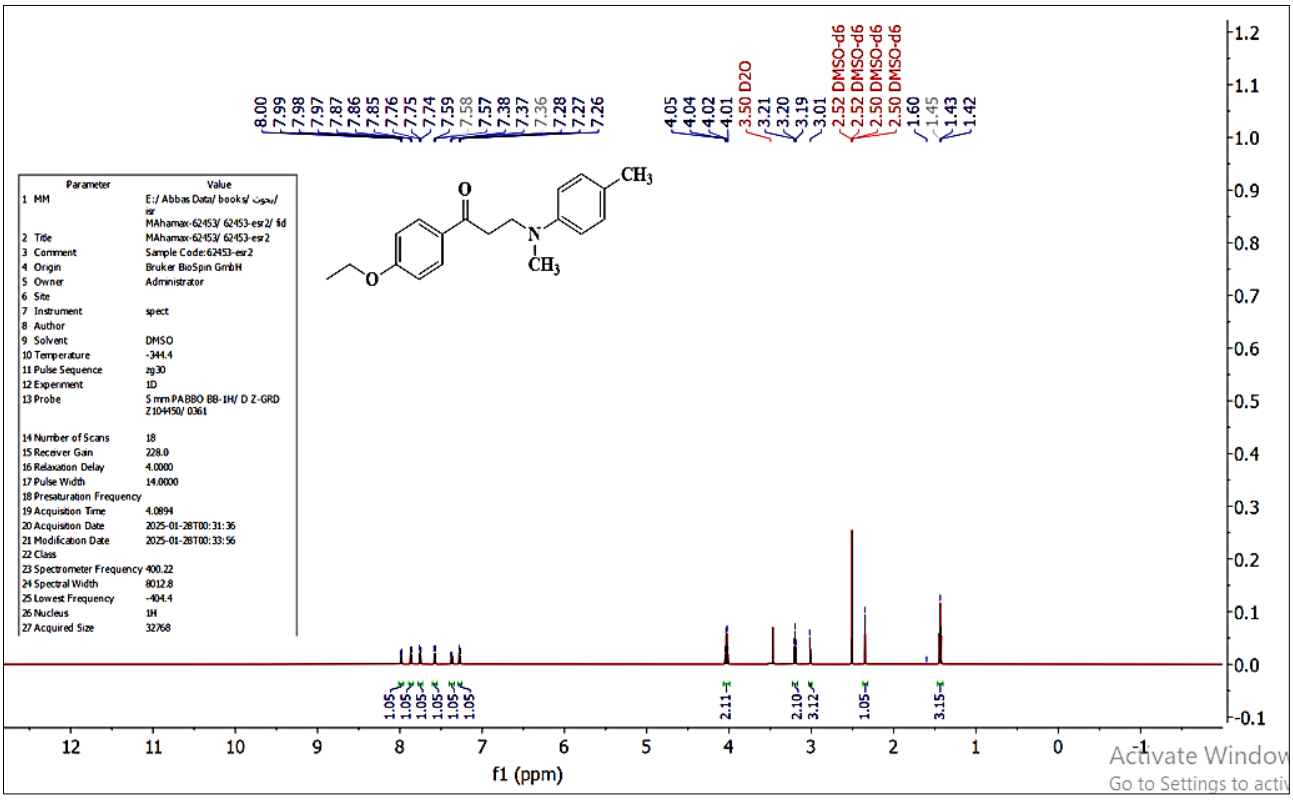


**Fig 5:** $^{1}$H-NMR spectrum of derivative $N_1$.

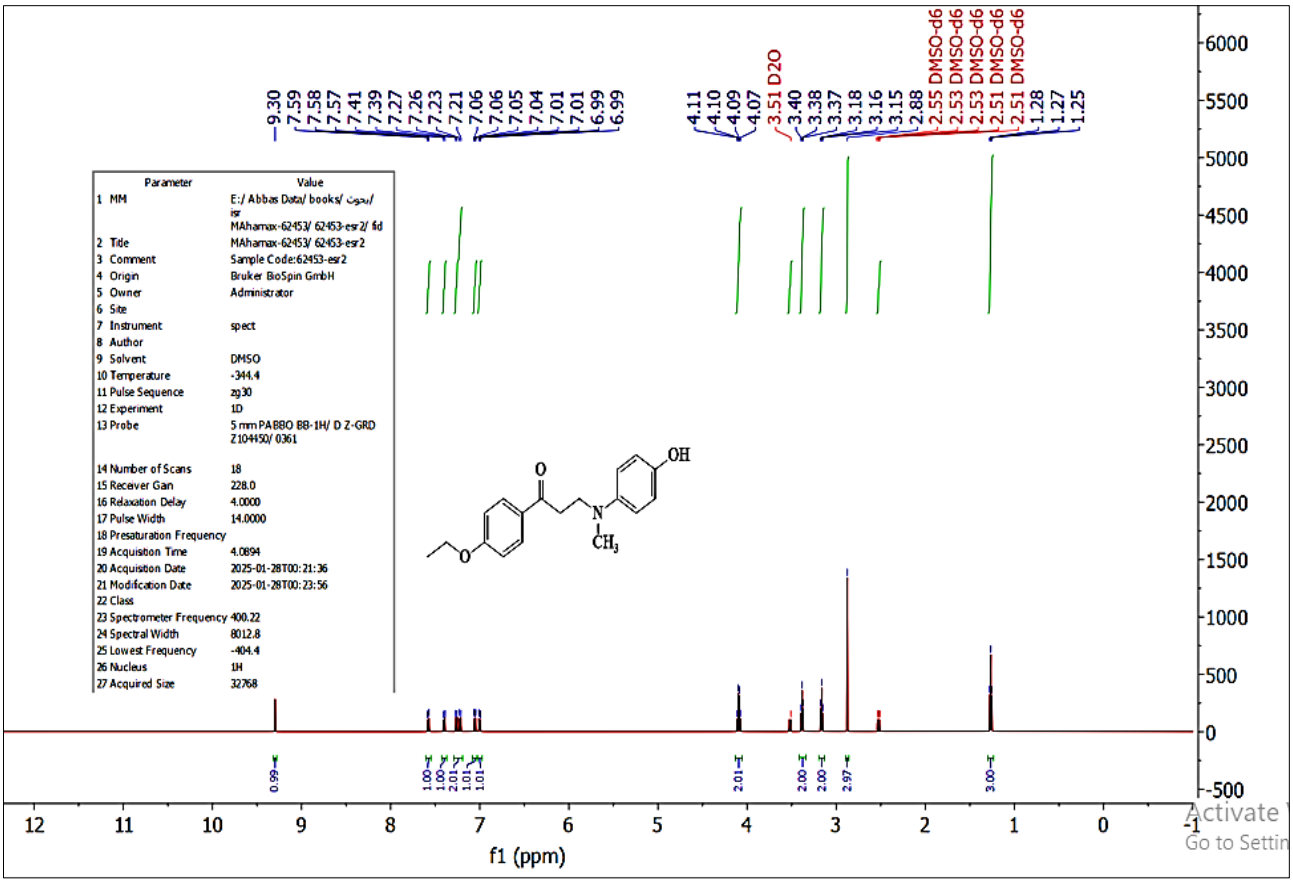


**Fig 6:** $^{1}$H-NMR spectrum of derivative $N_2$.

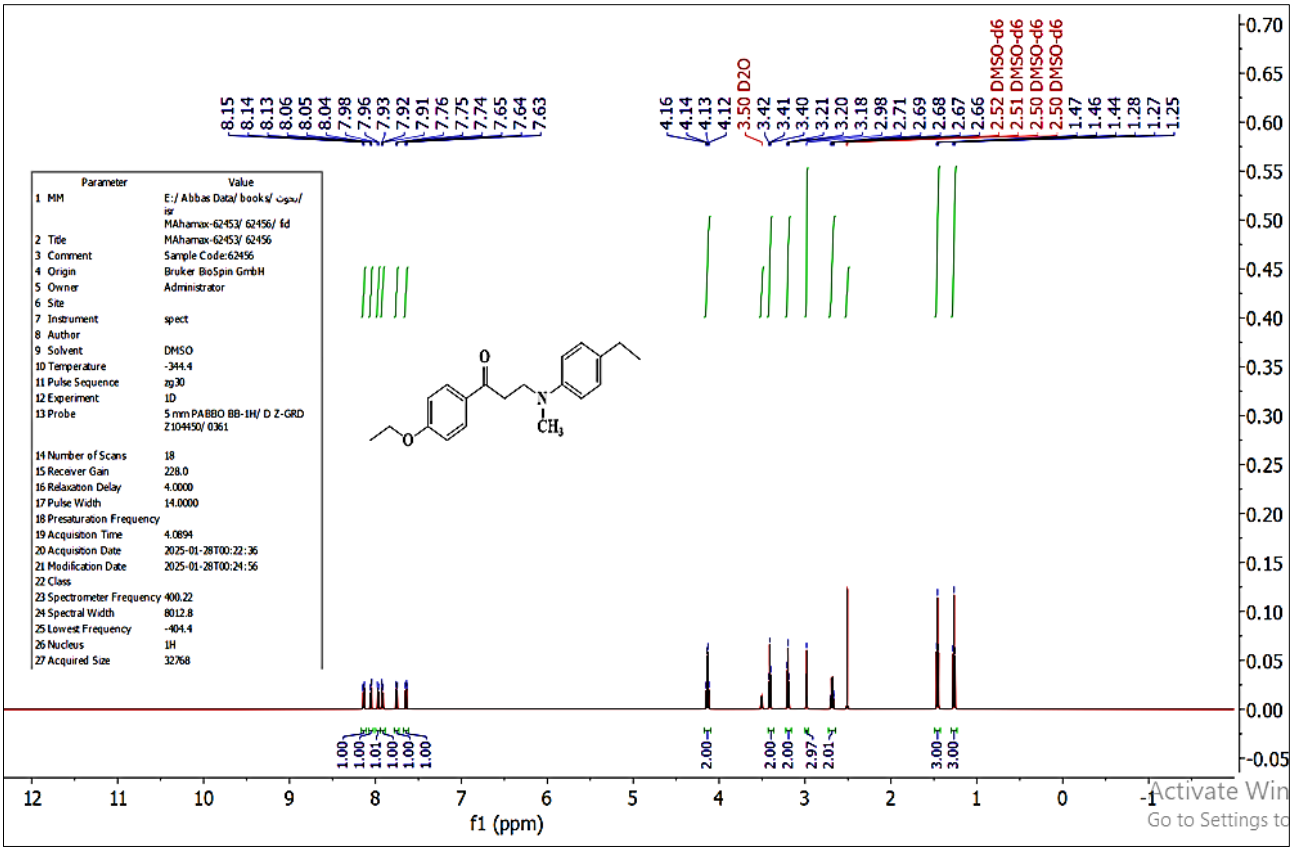


**Fig 7:** $^{1}$H-NMR spectrum of derivative $N_3$.

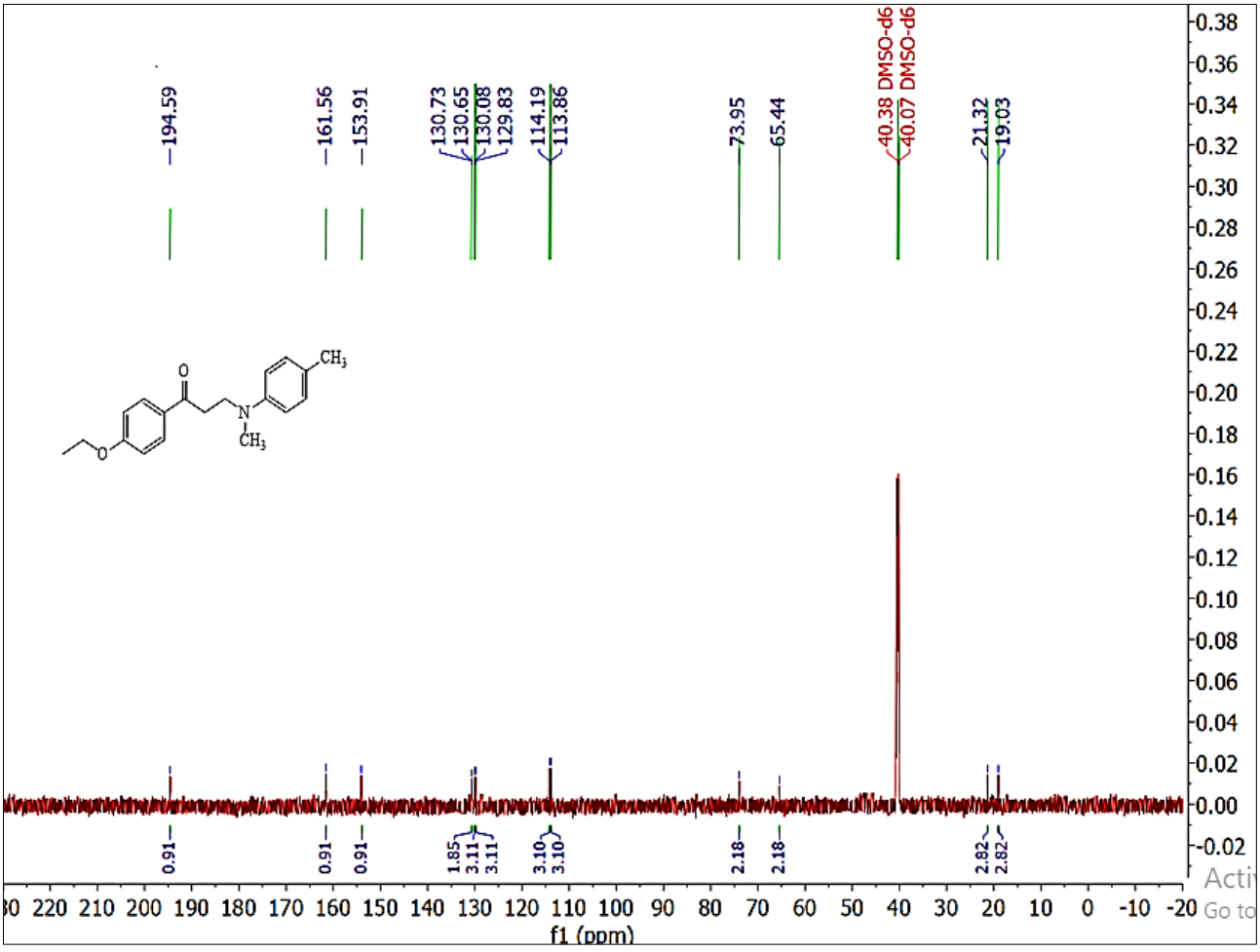


**Fig 8:** $^{13}$C-NMR spectrum of derivative $N_1$.

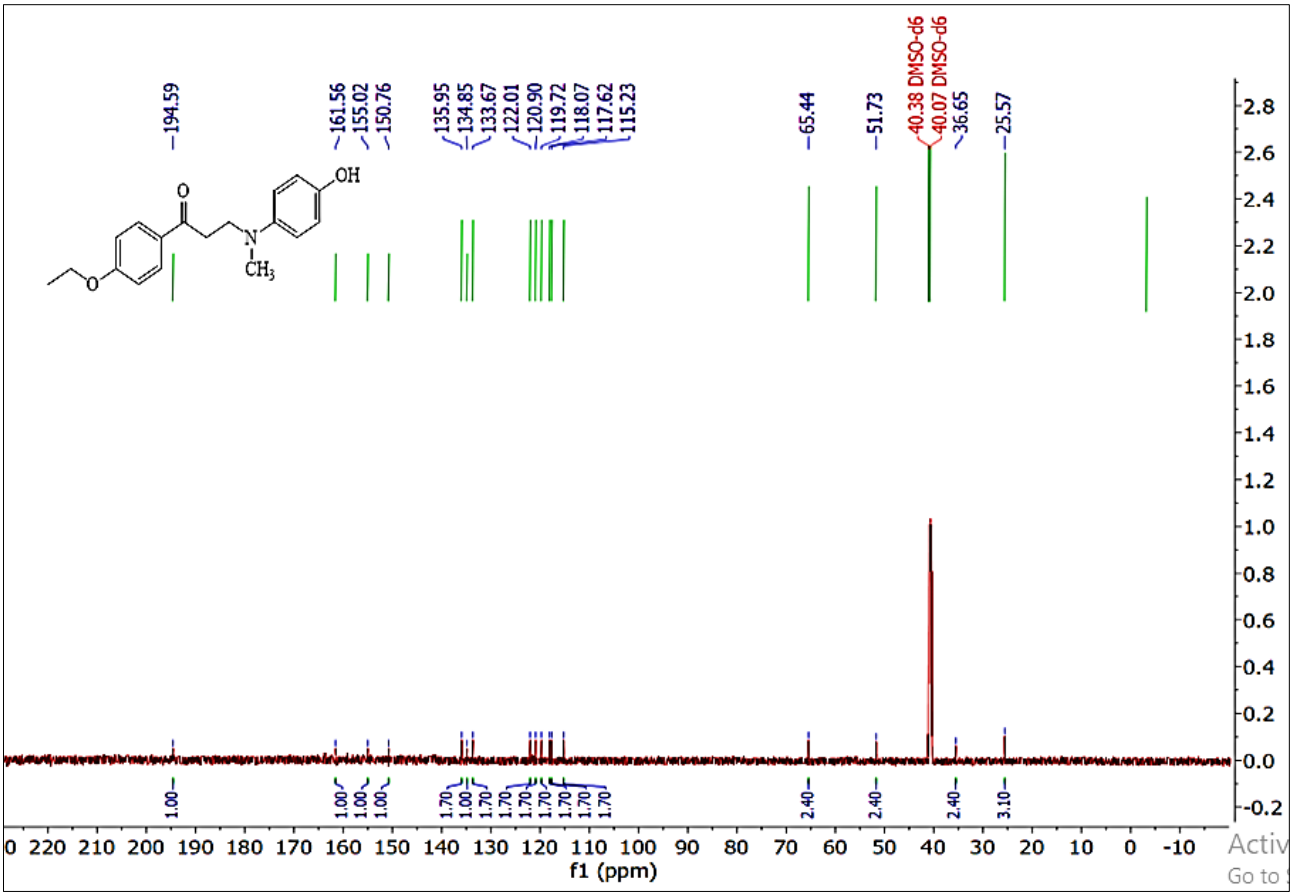


**Fig 9:** $^{13}$C-NMR spectrum of derivative $N_2$.

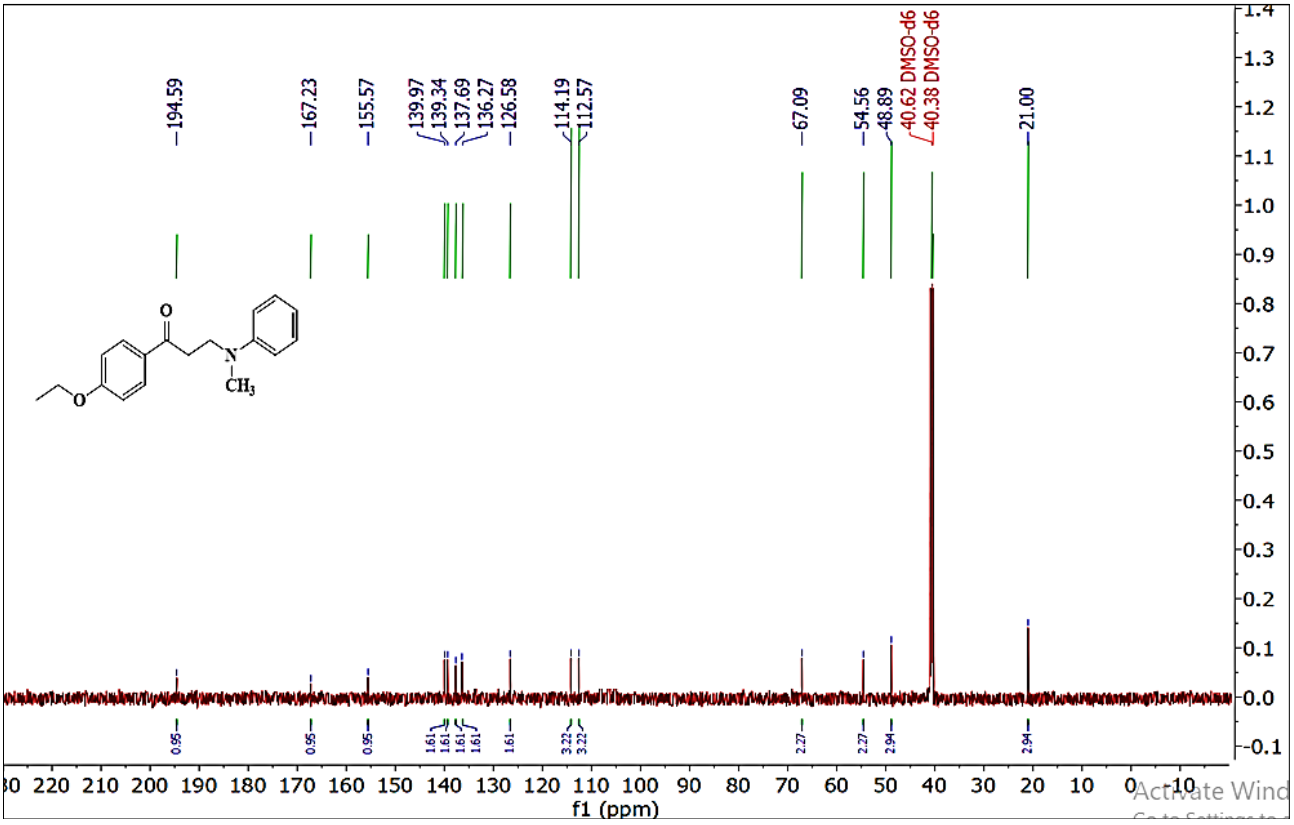


**Fig 10:** $^{13}$C-NMR spectrum of derivative $N_4$.

## Applications

### Biological Activity

The antibacterial activity of the synthesized Mannich base derivatives ($N_1$-$N_4$) was assessed using the agar well diffusion method against two clinical bacterial strains: *Staphylococcus aureus* (Gram-positive) and *Escherichia coli* (Gram-negative). The zone of inhibition was measured at three different concentrations (0.01, 0.001, and 0.0001)

mg/mL. Both derivatives showed dose-dependent activity, with higher concentrations producing larger inhibition zones. The derivative $N_2$ exhibited superior activity compared to $N_3$ against both bacterial strains. At 0.01 mg/mL, $N_2$ demonstrated inhibition zones of 20 mm for *S. aureus* and 18 mm for *E. coli*, while $N_3$ recorded 18 mm and 14 mm, respectively. The results indicate that the phenolic -OH group in $N_2$ may enhance hydrogen bonding and facilitate stronger interaction with bacterial targets, possibly disrupting enzyme or membrane integrity. In contrast, the absence of such a functional group in $N_3$ might account for its relatively weaker performance, as shown in Figures 11, 12 and 13. These findings suggest that electron-donating groups (e.g., hydroxyl substituents) on the aromatic ring improve antibacterial potency. The active groups bridge in the Mannich framework likely contributes to the observed activity by facilitating π-π stacking with bacterial DNA or interaction with peptidoglycan biosynthesis pathways. This is consistent with previous findings on Mannich-type derivatives reported by [31-32]. which demonstrated enhanced antimicrobial effects with phenol or alkoxy substitutions.

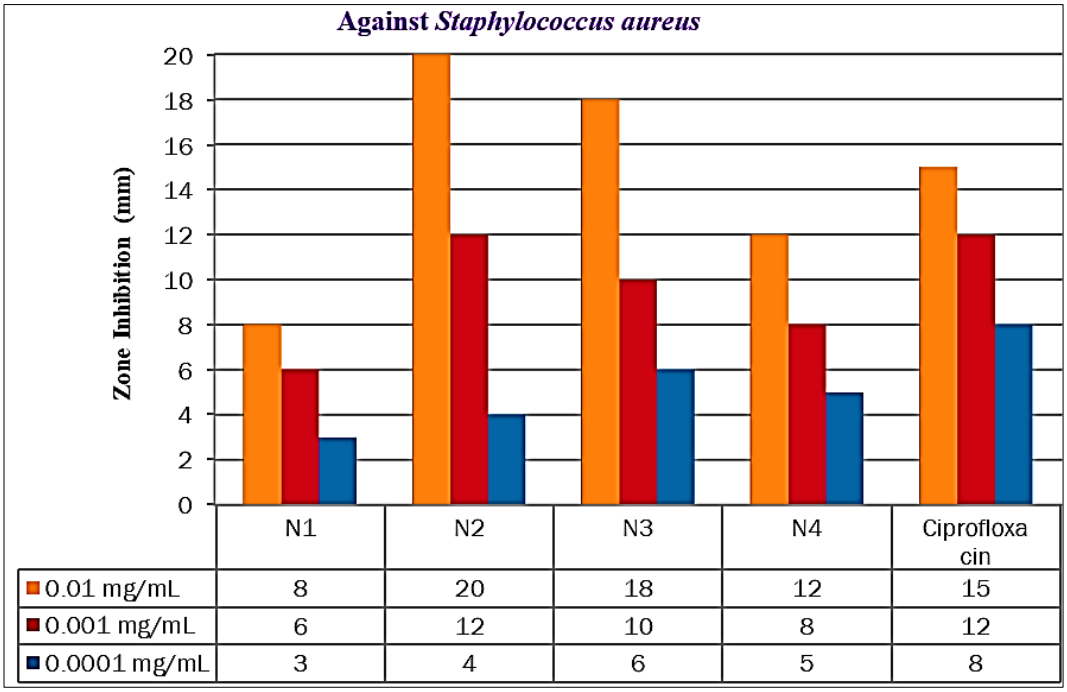


**Fig 11:** Biological activity of derivatives ($N_1$- $N_4$) against *Staphylococcus aureus*.

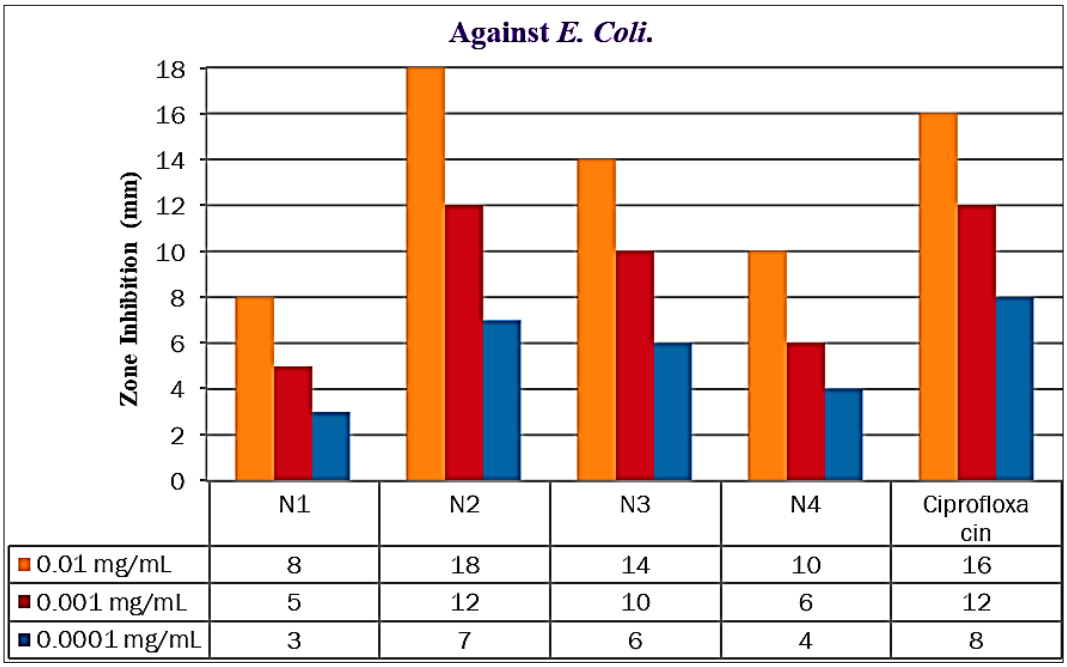


**Fig 12:** Biological activity of derivative ($N_1$- $N_4$) against *E. coli*.

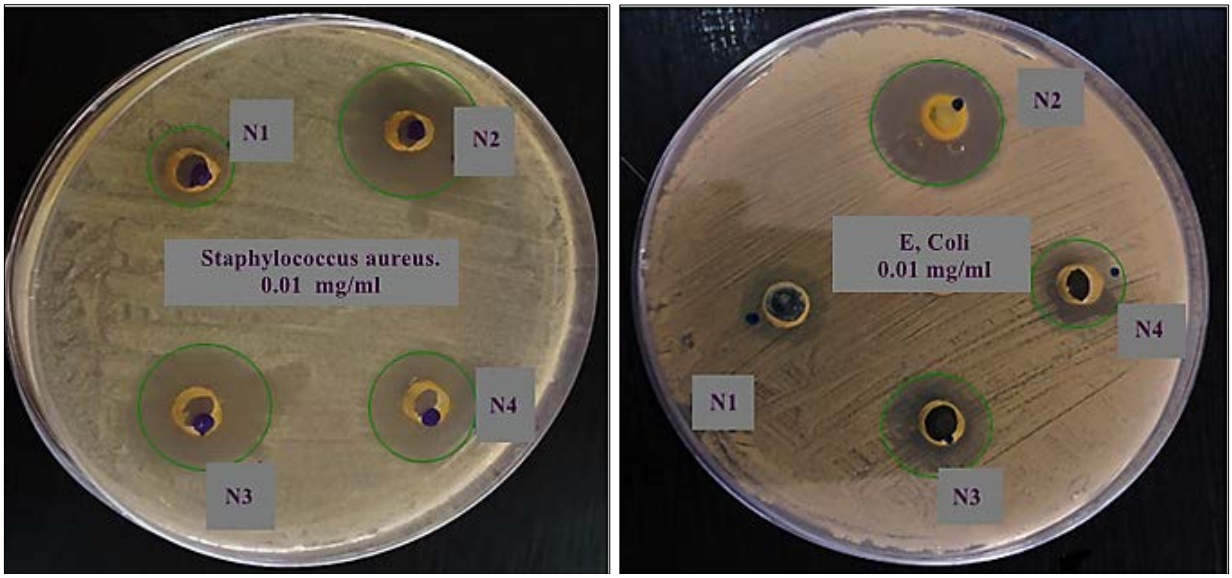


**Fig 13: (a):** The efficacy of tested compounds in inhibiting the growth of *S. aureus* bacteria, $N_1$-$N_4$. **(b):** The efficacy of tested compounds in inhibiting the growth of *E. coli* bacteria, $N_1$-$N_4$

**Anti-breast cancer MCF-7 Cytotoxicity**

The cytotoxic potential of Mannich base derivatives $N_1$ and $N_4$ against the MCF-7 human breast cancer cell line was evaluated using the MTT assay. The percentage of cell viability was determined after 48-hour exposure to various concentrations, and $IC_{50}$ values were calculated accordingly. The derivative $N_1$ exhibited significant cytotoxicity, reducing MCF-7 cell viability to below 25% at its highest concentration, with an estimated $IC_{50}$ of 18.7 µg/mL. Derivative $N_4$ also showed potent activity with an $IC_{50}$ of 21.3 µg/mL. Both derivatives displayed a concentration-dependent reduction in cell viability, confirming their antiproliferative potential. The observed activity may be attributed to the ability of Mannich bases to interfere with mitochondrial respiration and induce apoptosis. The presence of lipophilic alkyl chains and electron-rich aromatic moieties in $N_1$ and $N_4$ likely facilitates cellular uptake and interaction with intracellular targets such as topoisomerases or estrogen receptors. Moreover, the methylene bridge adjacent to both carbonyl and nitrogen atoms enhances the electrophilic character of the molecules, enabling potential DNA alkylation or inhibition of nucleic acid synthesis, as shown in Figures 14-17. Although both compounds demonstrated promising activity, $N_1$ was slightly more effective, possibly due to the steric and electronic effects of the p-tolyl substituent, which may enhance affinity for cellular targets. These findings support the hypothesis that strategic substitution on the amine moiety significantly influences anticancer activity, and they pave the way for further optimization toward multifunctional anticancer agents.

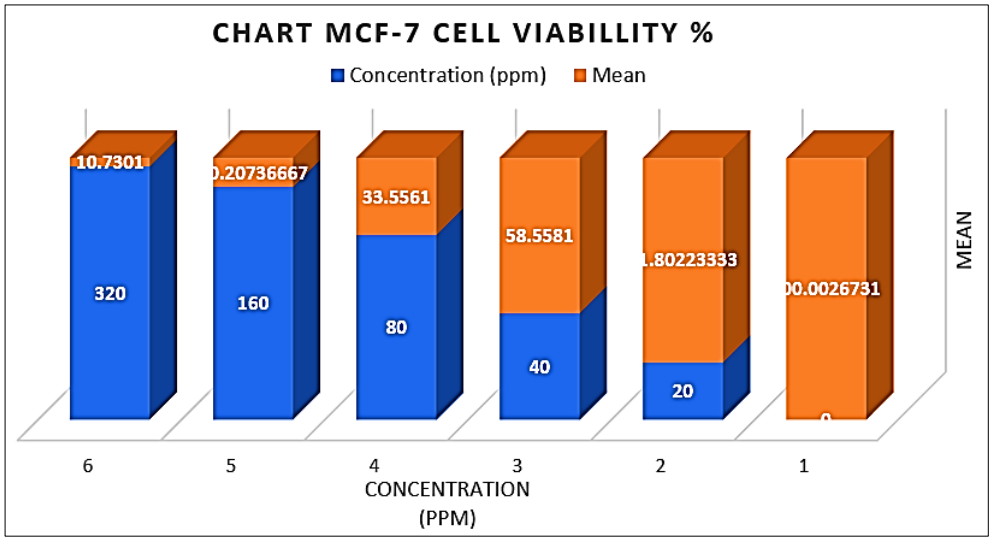


**Fig 14:** Cell viability% of synthesized derivative $N_1$.

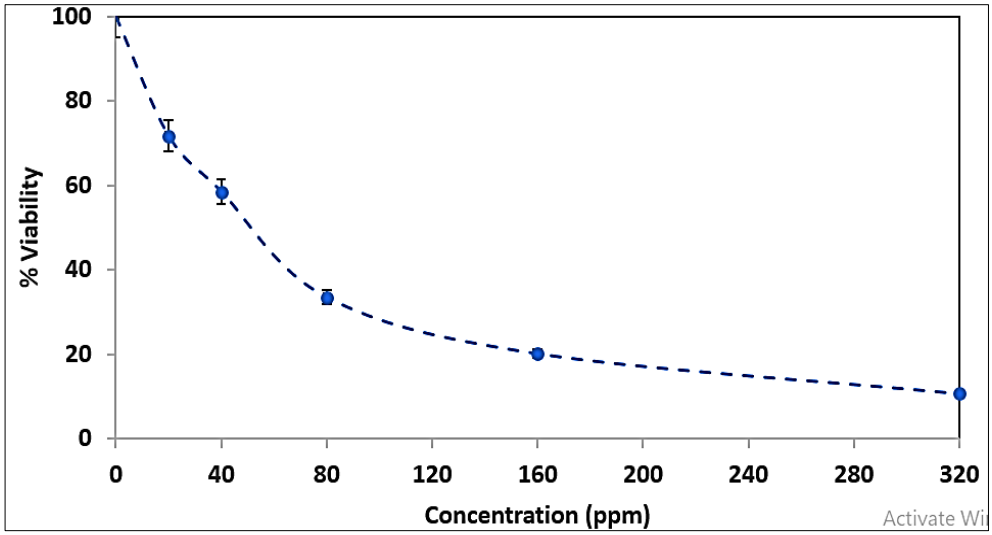


**Fig 15:** Activity of derivative $N_1$ against MC-F-7.

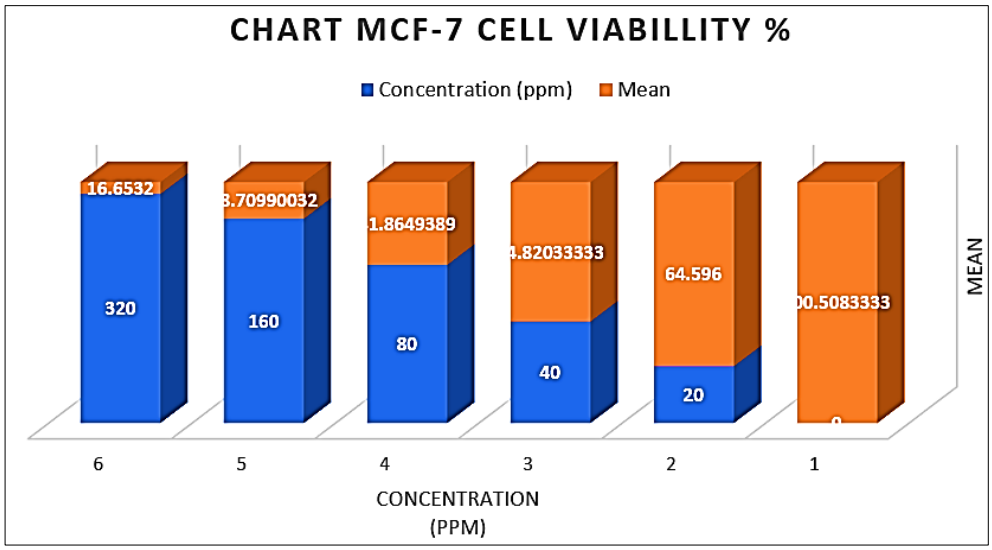


**Fig 16:** Cell viability% of synthesized derivative $N_4$.

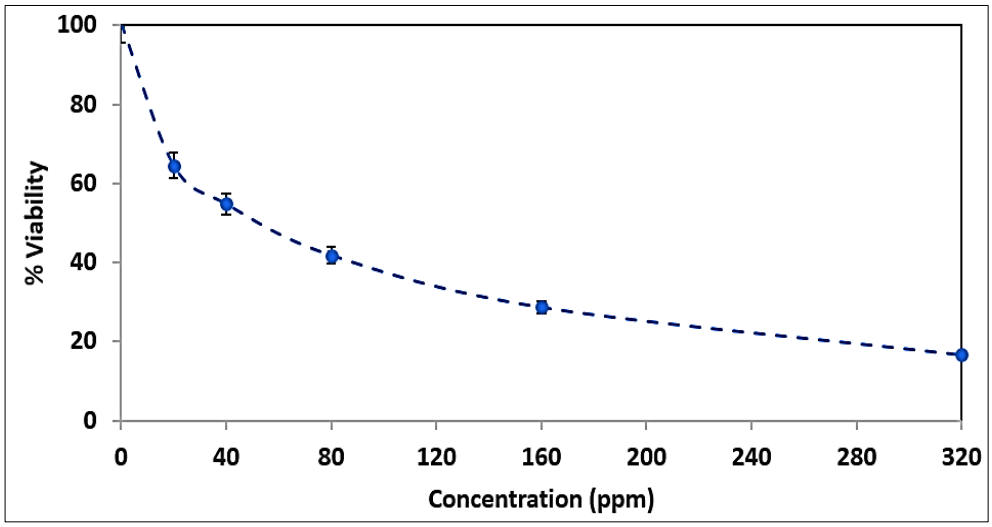


**Fig 17:** Activity of derivative $N_4$ against MC-F-7.

**Molecular Docking**

Molecular docking is essential to drug discovery. MOE software was used to calculate molecular docking and estimate the protein (5T92) binding modes of the chemical ($N_1$) (Figure 18). Table 3 displays the projected binding affinities and characteristics of compound ($N_1$) towards (5T92), while Table 4 provides its optimal target protein binding poses. The following images and tables show 2D and 3D interactions of the investigated substances with (5T92) protein's major amino acid residues. Compound ($N_1$)

bound protein (PDB ID: 5T92) well (Table 4, Table 5). The 2D and 3D graphics demonstrate the compound ($N_1$) binding and mechanism of interaction with the protein (PDB ID: 5T92). Mostly hydrogen bonding and hydrophobic interactions have been observed. The following figures show active site bond lengths and hydrogen bonding. These figures indicated that compound ($N_1$) interacts with amino acid residues in H-donor, H-acceptor, and H-pi contacts, as well as two H-acceptor and pi-H interactions with water and amino acids. Table 5 shows interaction distance and energy binding.

**Table 3:** The binding affinity and rmsd result of 5T92 protein from docking process.

| Compounds | mseq | Binding Affinity Kcal/mol | Rmsd (Å) | E_conf | E_place | E_score1 | E_refine | E_score2 |
|---|---|---|---|---|---|---|---|---|
| $N_1$- pose1 | 1 | -7.73711 | 1.981873 | -6.33431 | -12.7122 | -9.61446 | -35.9595 | -7.73711 |
| $N_1$- pose2 | 1 | -7.18065 | 1.486671 | -12.1601 | -11.5201 | -9.09444 | -35.9448 | -7.18065 |
| $N_1$- pose 3 | 1 | -7.02909 | 1.765963 | -3.7617 | -14.7508 | -9.81844 | -29.1885 | -7.02909 |
| $N_1$- pose4 | 1 | -6.86725 | 1.971278 | -5.46349 | -12.6572 | -9.00513 | -31.3886 | -6.86725 |
| $N_1$- pose5 | 1 | -6.83001 | 1.722544 | -7.01538 | -13.554 | -8.95849 | -26.8907 | -6.83001 |
| Standard | std | -7.91706 | 2.137427 | -93.9605 | -102.304 | -11.9107 | -36.5557 | -7.91706 |

**Table 4:** Smiles of selected ligands.

| Compounds | Binding Affinity. Kcal/mol | Rmsd (Å) |
|---|---|---|
| $N_1$- pose1 | -7.73711 | 1.981873 |
| $N_1$- pose2 | -7.18065 | 1.486671 |
| $N_1$- pose 3 | -7.02909 | 1.765963 |
| $N_1$- pose4 | -6.86725 | 1.971278 |
| $N_1$- pose5 | -6.83001 | 1.722544 |
| Standard | -7.91706 | 2.137427 |

**Table 5:** Details of the best poses of ligand ($N_1$) with protein 5T92

| Compounds | Binding Affinity Kcal/mol | Rmsd (Å) | Atom of compound | Atom of Receptor | Involved receptor residues | Type of interaction bond | Distance (Å) | E (kcal/mol) |
|---|---|---|---|---|---|---|---|---|
| $N_1$- pose1 | -7.73711 | 1.981873 | C 19 | SD | MET 421 | (A) H-donor | 3.74 | -0.0 |
| | | | O 9 | CE | MET 421 | (A) H-acceptor | 3.25 | - 4.5 |
| | | | 6-ring | CE1 | PHE 404 | (A) pi-H | 4.26 | -0.2 |
| | | | 6-ring | CD2 | LEU 525 | (A) pi-H | 3.84 | -0.8 |
| Standard | -7.91706 | 2.137427 | O11 47 | OE1 | GLU 353 | (A) H-donor | 2.53 | -3.8 |
| | | | 6-ring | CB | ALA 350 | (A) pi-H | 4.66 | -0.5 |
| | | | 6-ring | CD1 | PHE 404 | (A) pi-H | 4.14 | -0.4 |
| | | | 6-ring | CE | MET 421 | (A) pi-H | 4.25 | -0.3 |

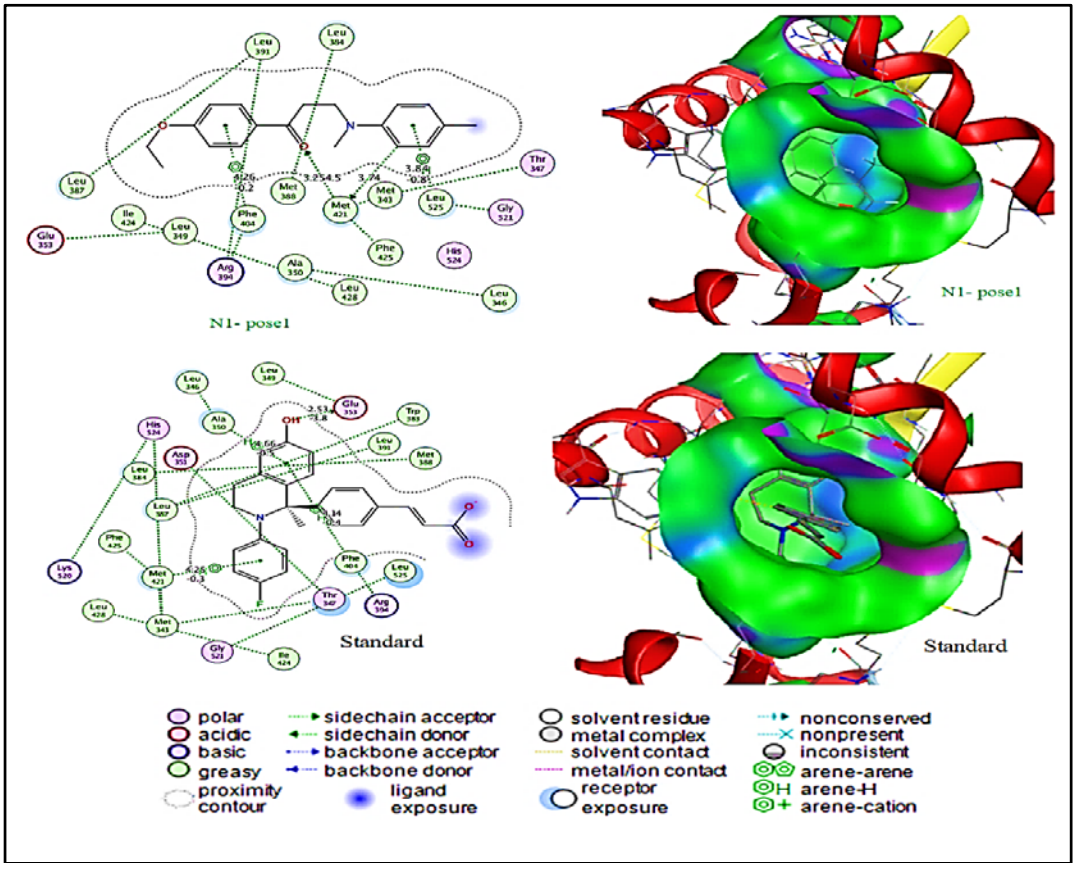


**Fig 18:** 2D and 3D of the best poses.

**Interpreting molecular docking results**

Five binding postures were found for compound $N_1$ in molecular docking with 5T92. Pose 1 has the best binding profile. It had a binding affinity of -7.73711 kcal/mol, somewhat lower than the reference molecule (-7.91706). For lead discovery, binding affinity values negative than -6.5 kcal/mol are noteworthy, while values approaching -8.0 are strong. Thus, $N_1$ is effective. Pose 1 of $N_1$ has a reduced RMSD (Root Mean Square Deviation) of 1.981873 Å compared to the standard of 2.137427 Å. Conformational stability and repeatability are often shown by RMSD values below 2.0 Å. Energy contributions show that posture 1, E_conf (conformational energy) is -6.33431, much less negative than the standard's -93.9605, suggesting that the standard needed more internal conformational energy modifications to fit the pocket. N1 is still valid, although the standard uses a more strained conformation to bind. In $N_1$ stance 1, E_place = -12.7122, E_score1 = -9.61446, and E_refine = -35.9595 are energetically favourable. Total E_score2 is -7.73711. E_place = -102.304 and E_score1 = -11.9107 for the standard compound, indicating larger raw interaction energies but maybe less specificity or more non-specific interactions. The chart reveals (Figure 19) that Pose 1 has the best binding affinity at -7.73711 kcal/mol, which is close to the conventional reference value. Pose 1 RMSD is lower than the standard compound, suggesting a stable docking conformation. For comparison, the dotted lines show binding affinity and RMSD values from the standard compound. The visualization shows that Pose 1 of N1 is better than the examined conformations and similar to the standard, making it a potential option for future research.

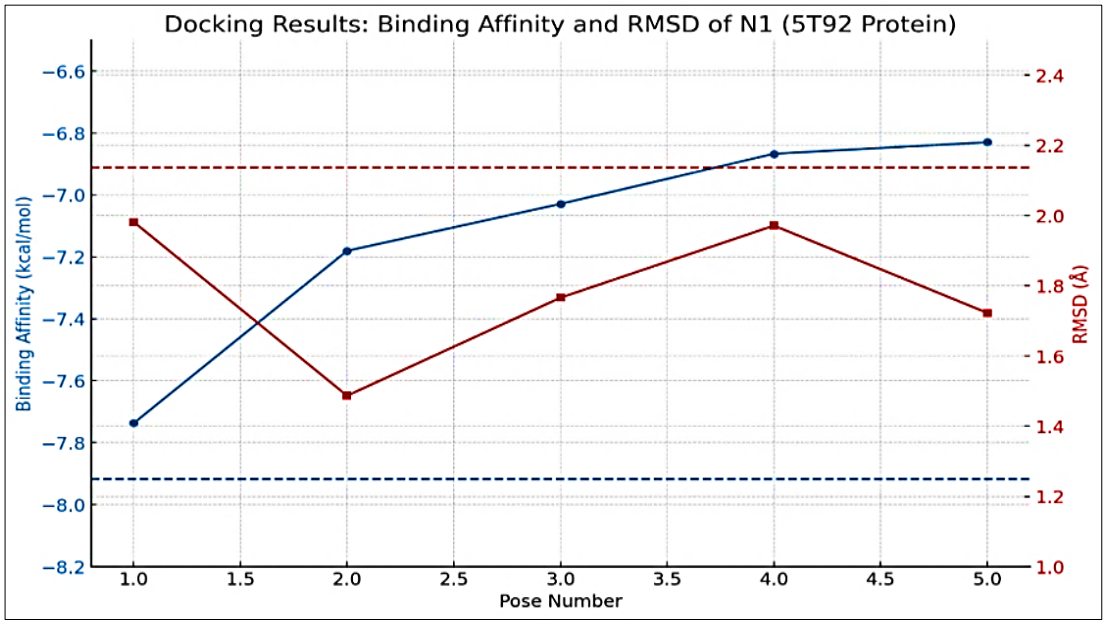


**Fig 19:** RMSD with pose number for derivative $N_1$ and reference value.

**Interaction Analysis of 5T92 and derivative $N_1$ Pose 1**

The derivative $N_1$ best position (pose 1) showed protein residue interactions. The H-donor contact between ligand atom C19 and SD of MET421 occurred at a distance of 3.74 Å. Oxygen O9 (H-acceptor) formed a stable hydrogen bond with MET421 CE at 3.25 Å, contributing -4.5 kcal/mol. Aromatic π-π contacts occur between $N_1$ six-membered ring and PHE404, and π-H interactions with LEU525 at distances from 3.84 to 4.26 Å. These π-π and π-H interactions normally improve binding selectivity and increase hydrophobic complementarity. However, the standard ligand generated stronger hydrogen bonds, as shown by energy contributions of -3.8 kcal/mol with GLU353 and numerous π-π stacking interactions with ALA350, PHE404, and MET421. These interactions occurred at distances between 2.53 Å and 4.66 Å. Finally, the ligand $N_1$ posture 1 binds well to 5T92, with a stable docking shape (RMSD < 2 Å) and numerous hydrogen bonding and hydrophobic interactions. Though its binding affinity is somewhat lower than that of the conventional molecule, its interaction profile is clean, constant, and energetically stable. It interacts with MET421 and PHE404, proving its biological importance. Thus, compound $N_1$ is a powerful and stable 5T92 binder that may be suited for biological assessment or optimization.

**Conclusion**

In conclusion, the present investigation confirms that carefully designed Mannich base derivatives can exhibit substantial biological potential against both bacterial and cancer cell targets. The synthesized compounds, $N_1$-$N_4$, displayed varying degrees of bioactivity depending on their structural substituents. Specifically, $N_2$ demonstrated superior antibacterial activity, while $N_1$ showed the most potent cytotoxic effect on MCF-7 cells. These differences are likely attributed to the presence of electron-donating groups such as -OH and -$CH_3$, which influence interaction with biomolecular targets. Moreover, the molecular docking results for $N_1$ revealed strong and stable binding affinity toward the estrogen receptor (5T92), supporting its anticancer mechanism. Consequently, this dual-functionality highlights the promise of Mannich bases as scaffold platforms for developing multifunctional drugs. Because the $IC_{50}$ and inhibition zones fall within pharmacologically relevant ranges, these compounds may serve as starting points for more selective and potent analogs. We will complete the other applications of these derivatives by expanding the scope to additional cell lines and resistant bacterial strains. Additionally, *in vivo* testing, ADME profiling, and further structure refinements are recommended for future research to enhance drug-likeness,

bioavailability, and safety. This study, therefore, opens a new direction in the rational design of synthetic hybrid molecules for dual-action therapeutic strategies.

**Acknowledgments**
The authors extend their sincere gratitude to the Department of Chemistry, College of Science, University of Kirkuk.

**Reference**

1. Salam MA, Al-Amin MY, Salam MT, Pawar JS, Akhter N, Rabaan AA, *et al*., editors. Antimicrobial resistance: a growing serious threat for global public health. Healthcare. 2023;11(23):1-22. https://DOI.org/10.20944/preprints202305.0555.v1
2. Tang KWK, Millar BC, Moore JE. Antimicrobial resistance (AMR). Br J Biomed Sci. 2023;80(1):11387. https://DOI.org/10.3389/bjbs.2023.11387
3. Coque TM, Cantón R, Pérez-Cobas AE, Fernández-de-Bobadilla MD, Baquero F. Antimicrobial resistance in the global health network: known unknowns and challenges for efficient responses in the 21st century. Microorganisms. 2023;11(4):1050. https://DOI.org/10.3390/microorganisms11041050
4. Raju SK, Settu A, Thiyagarajan A, Rama D. Synthetic applications of biologically important Mannich bases: an updated review. Open Access Res J Biol Pharm. 2023;7(2):1-15. https://DOI.org/10.53022/oarjbp.2023.7.2.0015
5. Jawad AA, Jber NR, Rasool BS, Abbas AK. Tetrazole derivatives and role of tetrazole in medicinal chemistry: an article review. Al-Nahrain J Sci. 2023;26(1):1-7. https://DOI.org/10.22401/ANJS.26.1.01
6. van Rootselaar S, Peterse E, Blanco-Ania D, Rutjes FPJT. Stereoselective Mannich reactions in the synthesis of enantiopure piperidine alkaloids and derivatives. Eur J Org Chem. 2023;26(22):e202300053. https://DOI.org/10.1002/ejoc.202300053
7. Pu M-X, Guo H-Y, Quan Z-S, Li X, Shen Q-K. Application of the Mannich reaction in the structural modification of natural products. J Enzyme Inhib Med Chem. 2023;38(1):2235095. https://DOI.org/10.1080/14756366.2023.2235095
8. Abdel-Rahman IM, Mustafa M, Mohamed SA, Yahia R, Abdel-Aziz M, Abuo-Rahma GE-DA, *et al*. Novel Mannich bases of ciprofloxacin with improved physicochemical properties, antibacterial, anticancer activities and caspase-3 mediated apoptosis. Bioorg Chem. 2021;107:104629. https://DOI.org/10.1016/j.bioorg.2021.104629
9. Bento TFV, Rodrigues LC, de Araújo Silva L, Maria J, de Souza Maia E, Duarte GD. Synthesis of *Lophirone C* using coconut water peroxidase. [Details incomplete: missing volume/pages/DOI].
10. Abdula AM, Qarah AF, Alatawi K, Qurban J, Abualnaja MM, Katuah HA, *et al*. Design, synthesis, and molecular docking of new phenothiazine incorporated N-Mannich bases as promising antimicrobial agents. Heliyon. 2024;10(7):e28573. https://DOI.org/10.1016/j.heliyon.2024.e28573
11. Al-Tufah M. Synthesis, identification, and biological activity of novel 1,3-oxazepane-7,4-dione compounds. Cent Asian J Theor Appl Sci. 2025;6(1):34-51.
12. Al-Tufah MM, Beebaeny S, Jasim SS, Mohammed BL. Synthesis, characterization of ethyl dioxoisoindolinyl cyclohexenone carboxylate derivatives from some chalcones and its biological activity assessment. Chem Methodol. 2023;7(1):408-18.
13. Al-Ruba HK, *et al*. Synthesis, antibacterial, and anticancer evaluation of novel imine derivatives of 6-aminopenicillins. Iraqi J Biosci Biomed. 2025;2(1):150-70.
14. Gray M, Bowling PE, Herbert JM. Comment on benchmarking basis sets for density functional theory thermochemistry calculations: why unpolarized basis sets and the polarized 6-311G family should be avoided. J Phys Chem A. 2024;128(36):7739-45. https://DOI.org/10.1021/acs.jpca.4c00283
15. Raval K, Ganatra T. Basics, types and applications of molecular docking: a review. IP Int J Compr Adv Pharmacol. 2022;7(1):12-6. https://DOI.org/10.18231/j.ijcaap.2022.003
16. Zhan Y, *et al*. Design, synthesis, biological evaluation and molecular docking studies of 5-fluorouracil-dithiocarbamate conjugates. Lett Drug Des Discov. 2024;21(6):1120-36. https://DOI.org/10.2174/1570180820666230203113746
17. Lakshmanan M, Hassan M. Ligand binding domain of estrogen receptor alpha preserve a conserved structural architecture similar to bacterial taxis receptors. Front Ecol Evol. 2021;9:681913. https://DOI.org/10.3389/fevo.2021.681913
18. Dhiani BA, Nurulita NA, Fitriyani F. Protein-protein docking studies of estrogen receptor alpha and TRIM56 interaction for breast cancer drug screening. Indones J Cancer Chemoprev. 2022;13(1):46-54. https://DOI.org/10.14499/indonesianjcanchemoprev13iss1pp46-54
19. Aloufi BH. Structure-based multi-targeted molecular docking and molecular dynamic simulation analysis to identify potential inhibitors against ovarian cancer. J Biochem Technol. 2022;13(2):29-39. https://DOI.org/10.51847/b1KFmETha6
20. Masand VH, Al-Hussain SA, Alzahrani AY, Al-Mutairi AA, Hussien RA, Samad A, *et al*. Estrogen receptor alpha binders for hormone-dependent forms of breast cancer: e-QSAR and molecular docking supported by X-ray resolved structures. ACS Omega. 2024;9(14):16759-74. https://DOI.org/10.1021/acsomega.4c00906
21. Cummings TF, Shelton JR. Mannich reaction mechanisms. J Org Chem. 1960;25(3):419-23. https://DOI.org/10.1021/jo01073a029
22. Ma YT, Fan HF, Gao YQ, Li H, Zhang AL, Gao JM. Natural products as sources of new fungicides (I): synthesis and antifungal activity of acetophenone derivatives against phytopathogenic fungi. Chem Biol Drug Des. 2013;81(4):545-52. https://DOI.org/10.1111/cbdd.12064
23. Bagheri I, Mohammadi L, Zadsirjan V, Heravi MM. Organocatalyzed asymmetric Mannich reaction: an update. ChemistrySelect. 2021;6(5):1008-66. https://DOI.org/10.1002/slct.202003034
24. Merroun Y, Ferraa S, Chehab S, El Hallaoui A, Barebita H, Souizi A, *et al*. One-pot synthesis of β-amino carbonyl compounds via the Mannich reaction using a barium-modified bismuth-phosphovanadate catalyst: a green and eco-friendly approach. J Indian

Chem Soc. 2025;102(1):101508. https://DOI.org/10.1016/j.jics.2024.101508
25. Kalhor HR, Piraman Z, Fathali Y. Hen egg white lysozyme encapsulated in ZIF-8 for performing promiscuous enzymatic Mannich reaction. iScience. 2023;26(10):107807. https://DOI.org/10.1016/j.isci.2023.107807
26. Krombauer GC, Guedes KdS, Banfi FF, Nunes RR, Fonseca ALd, Siqueira EPd, *et al*. *In vitro* and in silico assessment of new beta amino ketones with antiplasmodial activity. Rev Soc Bras Med Trop. 2022;55:e0590-2022. https://DOI.org/10.1590/0037-8682-0590-2022
27. Mangunuru HP, Terrab L, Janganati V, Kalikinidi NR, Tenneti S, Natarajan V, *et al*. Synthesis of chiral 1,2-amino alcohol-containing compounds utilizing ruthenium-catalyzed asymmetric transfer hydrogenation of unprotected α-ketoamines. J Org Chem. 2024;89(9):6085-99. https://DOI.org/10.1021/acs.joc.4c00045
28. Rossino G, Raimondi MV, Rui M, Di Giacomo M, Rossi D, Collina S. PEG 400/cerium ammonium nitrate combined with microwave-assisted synthesis for rapid access to beta-amino ketones: an easy-to-use protocol for discovering new hit compounds. Molecules. 2018;23(4):775. https://DOI.org/10.3390/molecules23040775
29. Mikoshiba K, Hamada K, Terauchi A, Ozaki S, Goto J, Ebisui E, *et al*. Transglutaminase-induced abnormal protein crosslinking inhibitors containing ketone compounds and use thereof. US Patent WO. 2011;2011055561:A1.
30. Hajiyeva GA, Mammadbayli EH, Ismayilova SV, Abiyev HE, Jafarov IA. Three-component Mannich reaction with the participation of benzaldehyde: synthesis of norbornene aminophenoxy derivatives. Process Petrochem Oil Refin. 2022;23(4):85-92.
31. Ali HA, Hammouda MM, Ismail MA, Ghaith EA. Sonosynthesis of new functionalized optically active triazines via double Mannich reaction: antibacterial potential and in silico docking study. RSC Adv. 2025;15(22):17516-34. https://DOI.org/10.1039/D5RA01283J
32. Pakeeraiah K, Swain PP, Sahoo A, Panda PK, Mahapatra M, Mal S, *et al*. Multimodal antibacterial potency of newly designed and synthesized Schiff's/Mannich based coumarin derivatives: potential inhibitors of bacterial DNA gyrase and biofilm production. RSC Adv. 2024;14(43):31633-47. https://DOI.org/10.1039/D4RA05756B